Available online at www.sciencedirect.com
SCIENCE DIRECT®
Earth and Planetary Science Letters 241 (2006) 438–453
EPSL
www.elsevier.com/locate/epsl

A new insight into the Hawaiian plume

Jianshe Lei *, Dapeng Zhao

Geodynamics Research Centre, Ehime University, Japan

Received 19 June 2005; received in revised form 22 November 2005; accepted 27 November 2005
Available online 5 January 2006
Editor: S. King

Abstract

Although many geochemical, geophysical and seismological studies have suggested that the Hawaiian mantle plume originates from the core–mantle boundary (CMB), so far no tomographic model shows a continuous image of the Hawaiian plume in the entire mantle because of the few seismic stations on the narrow Hawaiian island chain. Here we present a new tomographic image beneath Hawaii determined by using simultaneously 10 kinds of seismic phases, P, pP, PP, PcP, Pdiff, PKPab, PKPbc, PKiKP, PKKPab and PKKPbc, extracted from the data set compiled by the International Seismological Center. Of these phases, PKiKP, PKKPab and PKKPbc are, for the first time, attempted to use in the global seismic tomography. Our results show a slow anomaly beneath Hawaii ascending continuously from the CMB to the surface, implying that the Hawaiian plume indeed originates from the CMB. This image is improved notably over the previous results in the whole mantle, particularly in and below the middle mantle, suggesting that later phases, PP, Pdiff, PKP and particularly PKiKP, are of great importance for better imaging the Hawaiian plume. This slow anomaly is considered to be a plume conduit being tilted, which is likely caused by the mantle flow. This indicates that the position of the Hawaiian hotspot on the surface is not stationary, as evidenced by the recent paleomagnetic and numerical modeling studies.
© 2005 Elsevier B.V. All rights reserved.

Keywords: mantle plume; Hawaiian hotspot; P-wave tomography; global tomography; mantle and core phases

1. Introduction

Hotspots are characterized by topographic swell, higher temperature and recent volcanism with isotopic signatures distinct from those that characterize mid-ocean ridge or andesitic basalts [1–3]. Of all the hotspots, Hawaii is a well-known example. Hawaii is also one of the longest-lived hotspots and by far the strongest in flux, as measured by the topographic swell it created [1,2]. The volcanism responsible for creating the chain of the Hawaiian islands and seamounts (Fig. 1) is believed to mark the passage of the oceanic lithosphere over a mantle plume [4,5]. These Hawaiian islands form a linear chain with progressively increasing age away from the active region, perhaps reflecting a nearly stationary hotspot beneath the moving lithospheric plate. The formation of the Hawaiian hotspot may be caused by an upwelling mantle plume formed from instabilities at a hot thermal boundary layer in the Earth's mantle [1–5]. The core–mantle boundary (CMB) source of the Hawaiian hotspot has been commonly assumed [6–12], but the morphology of the mantle plume has long been debated because of the lack of seismic stations on the narrow Hawaiian volcanic chain.

* Corresponding author. Tel.: +81 89 927 8257; fax: +81 89 927 8167.
E-mail addresses: leijs@sci.ehime-u.ac.jp (J. Lei), zhao@sci.ehime-u.ac.jp (D. Zhao).

0012-821X/$ - see front matter © 2005 Elsevier B.V. All rights reserved.
doi:10.1016/j.epsl.2005.11.038

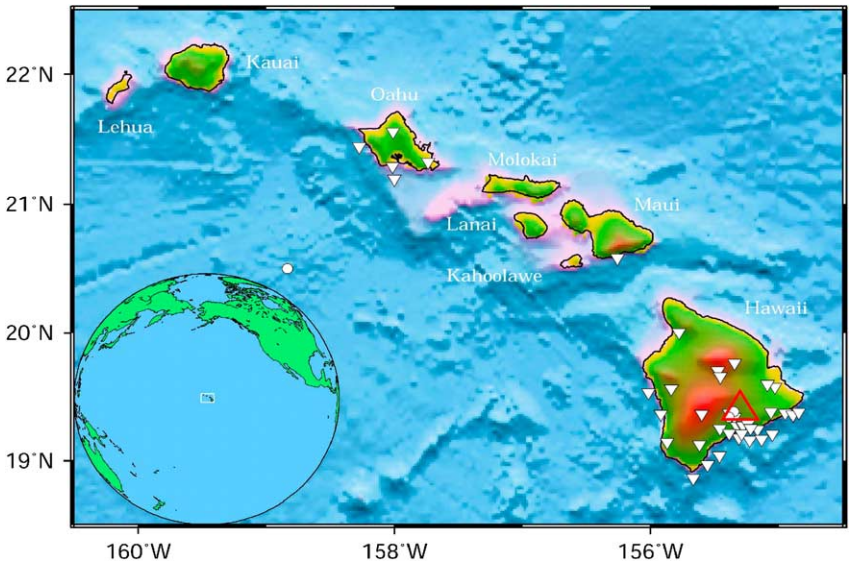

Fig. 1. Map of the study area. White triangles and white dots denote the seismic stations and earthquakes, extracted from the ISC bulletins, in and around the Hawaiian island chain. The hotspot (red triangle) is currently centered just southeast of Hawaii. The seismic stations are mainly located on the islands of Hawaii, Maui and Oahu. The insert map shows the location of the study area.

Many researchers have used geological, geochemical and geophysical approaches to study the Hawaiian hotspot [6–22]. Geochemical and gravity observations indicate the existence of a mantle plume beneath Hawaii [12,20–22]. A number of dynamic models have suggested possible plume–lithosphere interaction around Hawaii [2,17,21]. Teleseismic tomography revealed low velocity (low-V) anomalies beneath the Hawaiian islands in the upper mantle [19]. Analyses of Rayleigh wave data showed low velocity and thinning of the lithosphere beneath Hawaii [13–15]. An analysis of P to S converted seismic phase indicates the existence of a zone of very slow shear-wave velocity beneath Hawaii extending deeper into the lower mantle [17]. Waveform modeling and receiver function studies suggested that the Hawaiian hotspot may originate from the lower mantle [10,16,17]. Some results from diffraction wave and differential travel time tomography also displayed low-V anomalies existing in the lower mantle beneath Hawaii [9,23]. However, different global tomographic models showed different images of the Hawaiian plume. Fukao et al. [24] and Obayashi et al. [25] showed low-V anomalies beneath Hawaii limited to the middle mantle in depth. Montelli et al. [8] combined the International Seismological Center (ISC) data with the ray theory and travel times measured from waveforms using the kernel theory and concluded that the Hawaiian hotspot originates from the CMB, but the velocity structure of the lowermost mantle was less well resolved. Zhao [6,7] exhibited an intermittent low-V anomaly beneath Hawaii in his global tomographic models, perhaps because he used only mantle phases (P, pP, PP, PcP and Pdiff). So far no tomographic results show a continuous low-V cylinder beneath Hawaii extending from the CMB to the surface in the entire mantle.

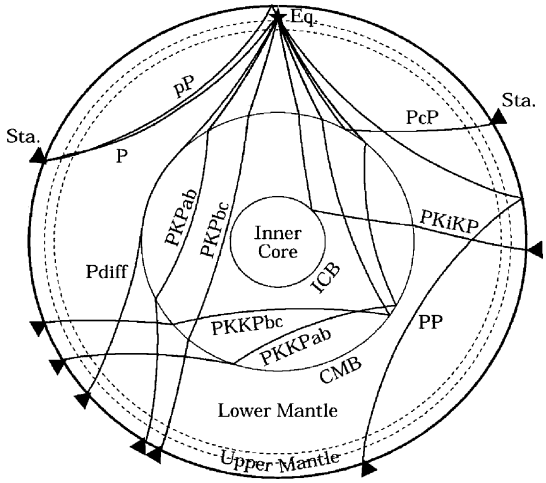

Fig. 2. Sketch illustration of ray paths used in this study. The rays are the direct P wave, depth phase (pP), surface reflected wave (PP), CMB reflected wave (PcP), outer core diffracted wave (Pdiff), outer core transmitted waves (PKPab and PKPbc), inner core reflected wave (PKiKP) and CMB underside reflected waves (PKKPab and PKKPbc). Star and inverted triangles denote earthquake and seismic stations. Two dashed lines denote the 410 and 660 km discontinuities, respectively.

Table 1
Mantle and core phases used in this study

Seismic phases	Number of data (1964–1998)	Number of data (1964–2003)	Delta ranges
P	783,024	1,026,776	0–96°
pP	36,017	48,868	30–100°
PP	8177	11,592	55–180°
PcP	4644	8698	25–40°, 45–70°
Pdiff	13,401	19,839	100–150°
PKiKP	5589	9488	100–115°
PKPab	5312	7918	155–180°
PKPbc	26,768	35,624	146–154°
PKKPab	157	587	105–120°
PKKPbc	515	2289	82–88°, 92–120°
Total	883,604	1,175,212	

Here we present a new global tomographic model obtained by applying the updated tomographic method of Zhao [6,7] to 10 kinds of seismic phases (Fig. 2). Our new model with all the phases shows a continuous low-V anomaly under Hawaii ascending from the CMB to the surface, which is a significant improvement over the previous results [6–8,24]. The images of other mantle plumes and subducted slabs are presented elsewhere [26]. In this paper, we focus on the resolution analysis and discussion of the low-V anomaly observed clearly beneath Hawaii.

2. Data and method

Later phases often sample the Earth's mantle structure not ordinarily sampled by the direct P waves in most portions of the mantle. Therefore, adding later phases is considered to be an effective way to improve the tomographic image, particularly for the Southern Hemisphere and oceanic regions where few seismic stations and events exist. In this work, in additional to the direct P wave, nine kinds of later phases (pP, PP, PcP, Pdiff, PKPab, PKPbc, PKiKP, PKKPab and PKKPbc) are included to image the mantle structure (Fig. 2). Comparing to the previous studies [6–8,24,27–29], three kinds of core phases (PKiKP, PKKPab and PKKPbc) have, for the first time, been used in the global seismic tomography. PKPdf and PKKPdf are not taken into account in this study because they pass through the inner core where strong anisotropy exists [30,31]. The data used were extracted from the ISC bulletins during 1964–1998 reprocessed by Engdahl et al. [32]. To identify all later-arriving phases of interest, a probabilistic method was used [32], which permits the use of selected later phases in calculating hypocenters by providing a basis for the relative weighting of phases. Each earthquake in our data set has more than 50 recordings and the focal depths were well constrained by pP depth phases. To avoid the effect of misidentified data and obtain a reliable tomographic image, we winnowed the data carefully, which is similar to the previous studies (e.g., [28,33–35]). Travel time residuals used in the inversion are confined to those less than 5.0 s. The total number of the data (1964–1998) used in the inversion amounts to 883,604. For details, see Table 1.

Fig. 3 illustrates the distribution of bounce points of PP on the surface, CMB legs of Pdiff, transmission points of PKP, PKiKP and PKKP through the CMB,

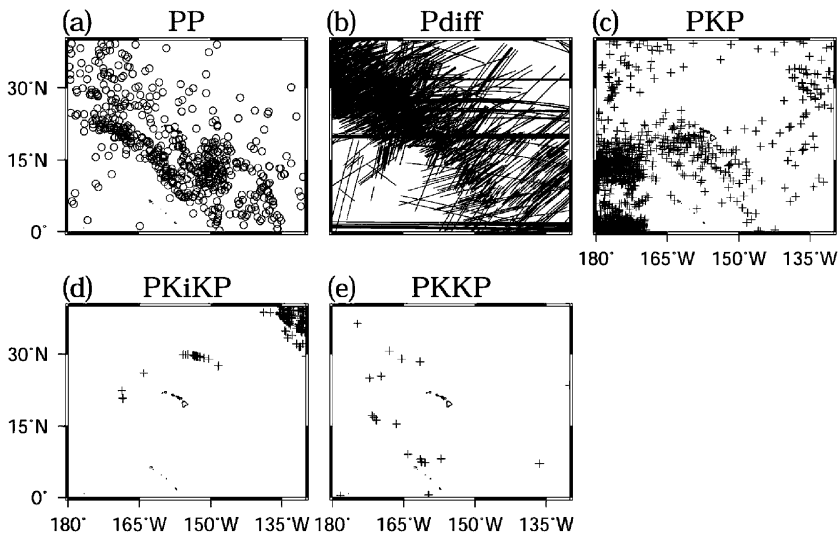

Fig. 3. Distributions of (a) bounce points (circles) of PP on the surface, (b) legs of Pdiff (lines) along the CMB, and transmission points (crosses) of (c) PKPab and PKPbc, (d) PKiKP and (e) PKKPab and PKKPbc through the CMB around Hawaii.

in and around Hawaii. Bounce points of PP are mainly distributed on the NW–SE orientation (Fig. 3a). The CMB legs of Pdiff have almost the same coverage with bounce points of PP (Fig. 3a and b). Transmission points of PKP have a good coverage around the Hawaiian islands except for the northeastern portion (Fig. 3c). The numbers of transmission points of PKiKP and PKKP are much smaller than those of PP, Pdiff and PKP. Transmission points of PKiKP are mainly distributed north of the Hawaiian islands in the Pacific Ocean (Fig. 3d) though most of them are distributed around the Pacific ring and Eurasia (Fig. 5e of [26]), while those of PKKP are focused on west of the Hawaiian islands (Fig. 3e). Bounce points of PcP on the CMB and those of pP on the surface are not shown here because of their few bounce points around Hawaii.

Fig. 4 shows the distribution of cap-averaged travel time residuals around Hawaii. Cap sizes are 2.5° × 2.5°. PP phases show a mixture pattern of positive and negative residuals from southeast to northwest (Fig. 4a). Pdiff phases have an obvious pattern showing most positive and few negative residuals (Fig. 4b). PKP phases display a positive residual pattern (Fig. 4c), but their amplitudes are smaller than those of Pdiff phases. The distribution of Pdiff and PKP residuals suggests that there are some low-V anomalies around Hawaii in the lowermost mantle. PKiKP and PKKP phases show some prominent positive residuals observed north of Hawaii, which are as large as 3–4 s (Fig. 4d and e). These results suggest that low-V anomalies will appear more obviously under Hawaii in the lower mantle after adding PKiKP and PKKP phases though the number of the two phases is limited. For details, see Section 4.3.

Fig. 5 shows the distribution of different types of rays projected on the north–south vertical cross-section. To see the distribution of the rays under Hawaii clearly, we also illustrated the rays of the direct P, pP and PP waves within 10° of the profile (Fig. 5d–f). The direct P phase has much more rays than other phases, but the P rays have a distribution of a mountain-like shape under Hawaii above 1000 km depth and a relatively poor coverage around 1500 km depth, and are almost horizontal below 2000 km depth (Fig. 5a and d). The pP ray distribution is similar to that of P rays in the global scale. Both P and pP rays are not so useful for imaging the area away from the Hawaiian islands in and above the mantle transition zone (Fig. 5a, b, d and e). However, PP rays can compensate the shortcoming of the P and pP ray coverage above 1500 km depth (Fig. 5c and f). PcP and PKKP have much fewer rays around the Hawaiian islands (Fig. 5g and k). Pdiff and PKP have good coverages in the lowermost mantle (Fig. 5h and i), and most of rays come from earthquakes through the range to seismic stations distributed along the Pacific ring. In addition, there are some Pdiff rays in Fig. 5h coming from the Hawaiian islands, while no PKP arrival times are recorded by the Hawaiian seismic stations in our data set (Fig. 5i). Some PKiKP rays come from the Hawaiian islands, and others in the northern

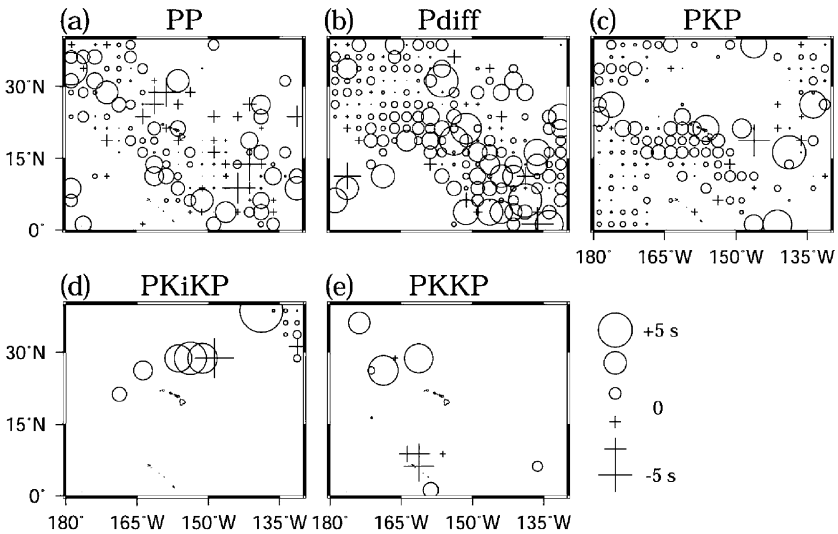

Fig. 4. Distribution of cap-averaged travel time residuals for PP (a), Pdiff (b), PKP (c), PKiKP (d) and PKKP (e) around Hawaii. Residuals of PP and Pdiff rays are expressed at their bounce points on the surface and mid-points of the CMB legs, respectively, while those of PKP, PKiKP and PKKP rays are expressed at their transmission points. The residuals are averaged over the points within a cap of 2.5° × 2.5° and plotted in the center of the cap. Circles and crosses denote the positive and negative residuals, respectively. The scale for residuals (in sec) is shown on the right of (e).

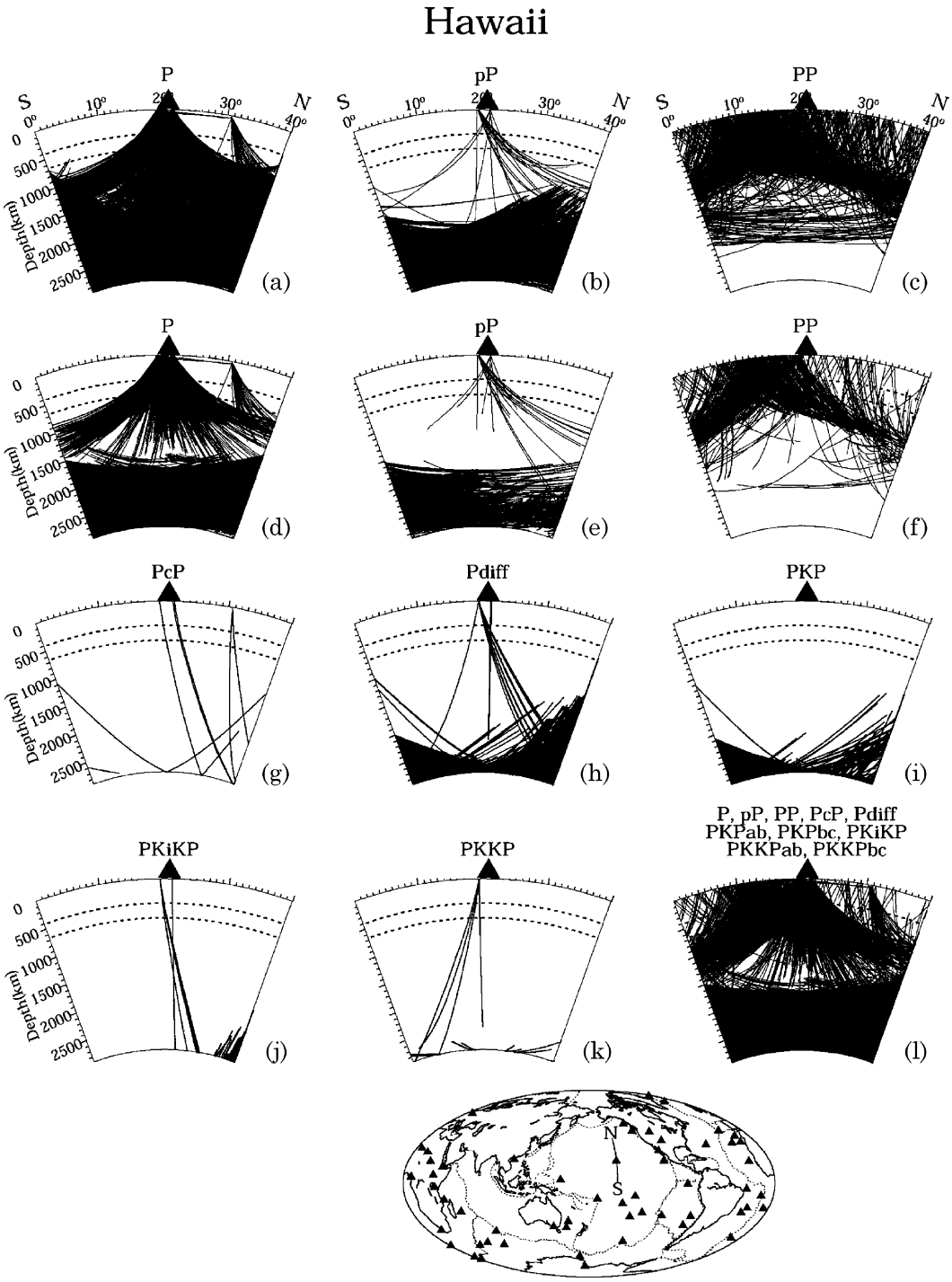

Fig. 5. Distribution of seismic rays projected on the north–south vertical cross-section passing through the Hawaiian hotspot. (a)–(c) and (g)–(k) illustrate the rays passing through the area shown in Fig. 3, while (d)–(f) delineate the rays within 10° of the profile so that the direct P, pP and PP rays under Hawaii can be seen clearly. The rays in (l) are a combination of those in (d)–(k). Seismic phases are listed at the top of each panel. Two dashed lines denote the 410 and 660 km discontinuities. Location of the profile is shown on the insert map. Triangles on the map denote the hotspots in the world.

portion are some segments of rays from earthquakes through the range to seismic stations around Northeast and Southwest Pacific (Fig. 5j), which may be also an important constraint in imaging the Hawaiian plume in the lowermost mantle. When all phases are plotted, the ray coverage is much better under Hawaii throughout

the entire mantle, though it is still relatively poor in the middle mantle (Fig. 5l). Pdiff, PKP and particularly PKiKP can enhance the ray crisscrossing with the direct P and pP phases below 2000 km depth. The former is relatively vertical at these depths, while the latter is nearly horizontal. Nevertheless, adding later phases can improve crisscrossing of rays significantly in the entire mantle, which will be further discussed in Section 4.3.

A 3-D ray tracing technique [36,37] was used, which combines the pseudo-bending algorithm [38] and Snell's law. Based on Zhao [7], in this study, we newly added five kinds of core phases (PKPab, PKPbc, PKiKP, PKKPab and PKKPbc) in the tomographic inversion. Travel time residuals were calculated by using the iasp91 1-D velocity model [39]. Topography and bathymetry (available online at http://mahi.ucsd.edu/Gabi/rem.html) were taken into account in the calculation of pP and PP. The travel times were corrected for the Earth's ellipticity [40]. 3-D grid nodes were set up in the model to express the Earth's structure, which have a grid spacing of $6^\circ \times 6^\circ$ laterally and 35–250 km in depth. Velocity perturbations at the grid nodes were taken as unknown parameters. The velocity perturbation at any point in the model was obtained by linearly interpolating those at eight grid nodes around that point. A system of observation equations was constructed and the LSQR algorithm [41] with damping and smoothing was used to conduct inversions [6,7].

3. Results and resolution analyses

A very slow anomaly is visible around the Hawaiian hotspot at all depth levels of the mantle, and the morphology, location and amplitude of this slow anomaly change with depth (Fig. 6). This slow anomaly biases toward the west and has a similar shape at different depths in the upper mantle (Fig. 6a–d), while below the mid-mantle it shifts towards the northeast gradually (Fig. 6g–i). In the lower mantle, the anomaly is reduced in size and amplitude with depth (Fig. 6e–h), but at the base of the mantle it becomes stronger again (Fig. 6i), which suggest that the reduction in the amplitude of the anomaly with depth may be due to a decrease in $\mathrm{d}V/\mathrm{d}T$ (V, velocity; T, temperature) with pressure, while the subsequent increase in the D'' layer region may be due to a reversal of the trend in $\mathrm{d}V/\mathrm{d}T$, which might be related to temperature anomalies instead of a transformation to post-perovskite under Hawaii because the post-perovskite transition needs a very large positive Clapeyron slope (e.g., [42,43]). This is different from the cold subduction areas, such as Alaska and Central America.

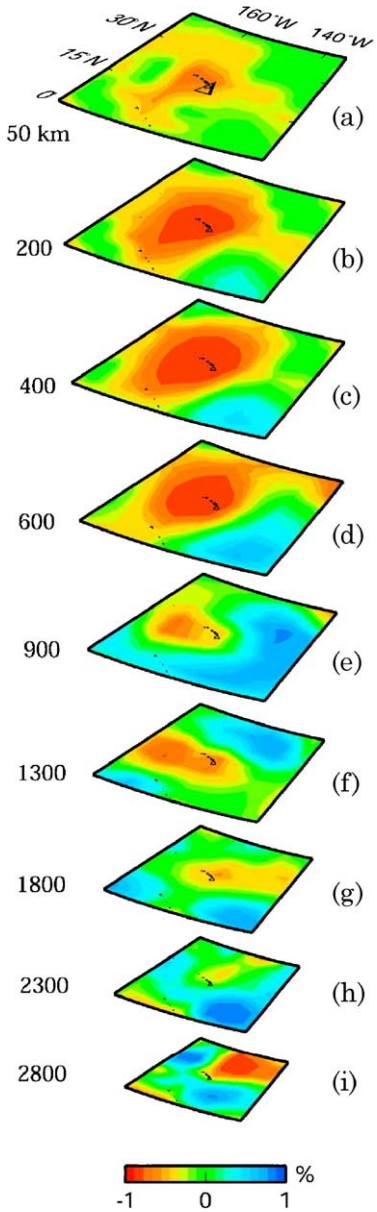

Fig. 6. P-wave tomographic images in map view around the Hawaiian hotspot at some representative depths. The depth of each layer is noted on the left of each map. The size of each map is decreased with depth to keep the scale constant. Red and blue colors denote slow and fast velocities, respectively. The velocity perturbation scale (in %) is shown at the bottom, relative to the iasp91 1-D Earth model [39]. The triangle denotes the Hawaiian hotspot.

Fig. 7a shows our tomographic results along a north–south vertical cross-section passing through the Hawaiian hotspot when all phases are used, while the CMB topography is not considered. An obvious low-V anomaly exists continuously from the CMB to the surface in the entire mantle. This slow anomaly is imaged as an inclined cylinder, which is possibly af-

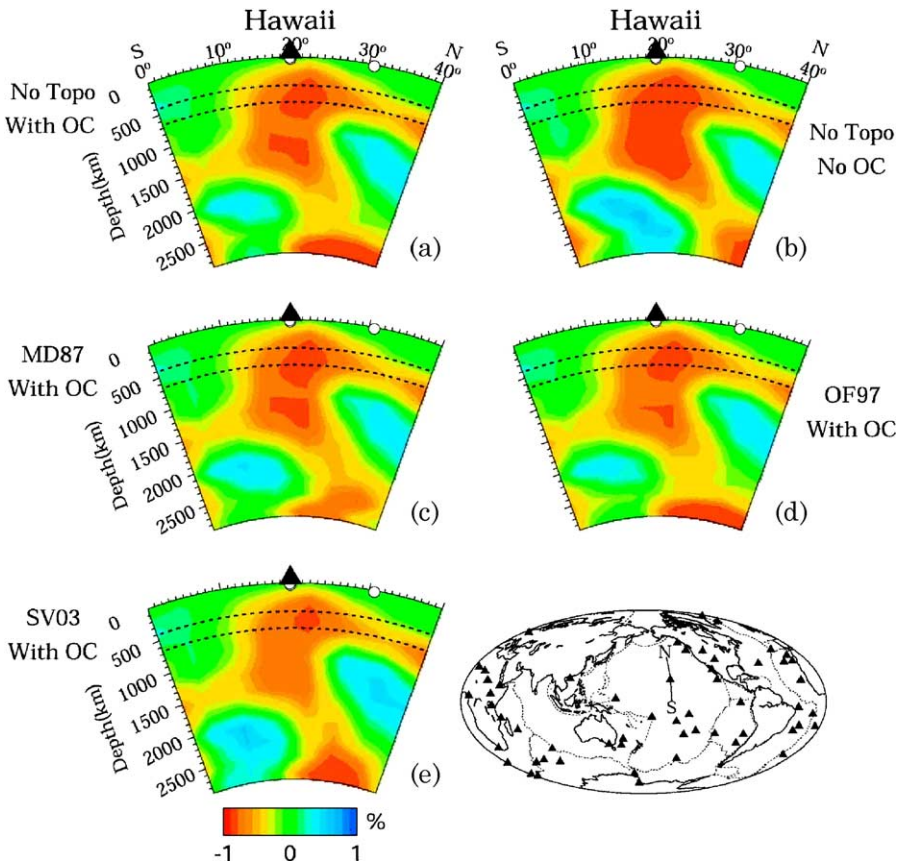

Fig. 7. P-wave tomographic images along the north–south vertical cross-section beneath the Hawaiian hotspot when all phases are used. (a) The image obtained without the CMB topography and with the outer core structure included in the inversion; (b) the image obtained without the CMB topography and without the outer core structure included in the inversion; (c–e) the images obtained with the outer core structure included in the inversion and with three CMB topographic models taken into account. These three models are MD87 [33], OF97 [46] and SV03 [35], respectively. The two dashed lines denote the 410 and 660 km discontinuities. Red and blue colors denote slow and fast velocities, respectively. The velocity perturbation scale (in %) relative to the iasp91 1-D Earth model [39] is shown at the bottom. The insert map shows the location of the cross-section. The triangles denote the hotspots in the world. White dots denote the earthquakes occurred within 250 km of the profile.

fected by the mantle convection. In the D'' layer, it shows a very strong slow anomaly, which is likely to be the source of the Hawaiian plume.

To confirm the main features beneath the Hawaiian hotspot, we have carried out two kinds of resolution tests to assess the adequacy of ray coverage and evaluate the resolution (e.g., [6,7,44]). One is checkerboard resolution tests for evaluating the spatial resolution of tomographic image in the entire study area (Fig. 8). The other is synthetic tests for examining the resolvability of the structure right beneath the Hawaiian hotspot (Fig. 9). The checkerboard resolution test is just a special form of the synthetic test. The difference between them is just in the input model. The resolution in the middle and lower mantle is much better than that in the upper mantle (Fig. 8). Such significant improvement over the previous studies [6,7] around Hawaii is attributable to a large number of later phases used. The effect of later phases on the tomographic image around Hawaii is discussed in Section 4.3.

A number of synthetic tests have been conducted by changing the diameter and morphology of slow anomalies beneath the Hawaiian hotspot. Six of such tests are illustrated in Fig. 9. In the first three tests, slow anomalies of up to -1% are put from the surface to a depth of 660 km, 1700 km and the CMB, respectively (Fig. 9a, c and e). In the following two tests, two patches of slow anomalies of up to -1% are put beneath the Hawaiian hotspot from the surface to 1700 km depth and from 2600 km depth to the CMB, respectively (Fig. 9g and i), but there exist some differences in the amplitude of velocity anomalies between 1700 and 2600 km depths: in the fourth test, no velocity anomalies are put (Fig. 9g), while in the fifth test velocity anomalies of up to

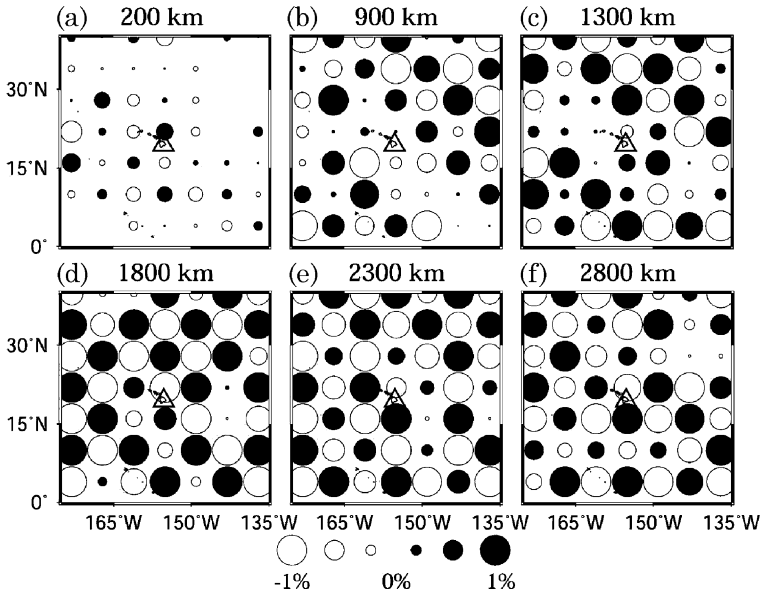

Fig. 8. Results of a checkerboard resolution test in map view around the Hawaiian hotspot at some representative depths. The depth of each layer is noted at the top of each map. Open and solid circles denote low and high velocity anomalies, respectively. The velocity perturbation scale (in %) is shown at the bottom. The triangle denotes the Hawaiian hotspot.

−0.5% are put (Fig. 9i). The purpose of these two tests is to confirm whether the slow anomalies between 1700 and 2600 km depths are real. The sixth one is that slow anomalies with a similar pattern as the real image are put from the surface to the CMB (Fig. 9k), to confirm whether the southward inclination of the mantle plume and southward extension of slow anomalies around 1500 km depth are real. The output models have almost the same patterns as the input models though there are some differences between them in the amplitude. Slow anomalies in the upper mantle are reconstructed with slight smearing to the lower mantle (Fig. 9b) and the amplitude of slow anomalies around 1500 km is less well recovered (Fig. 9d, f, h, j and l), suggesting that there is a relatively weak crisscrossing of rays there (Fig. 5l). Nonetheless, the main features of our tomographic result ((Figs. 6, 7, 10i or 12i and 13a)) have been demonstrated to be robust by our extensive checkerboard resolution and synthetic tests (Figs. 8 and 9). In particular, the slow patches from 1700 to 2600 km depths are real rather than a vertical leakage considering the results of the synthetic tests (Fig. 9e–j).

4. Discussion

4.1. Effect of the outer core structure

It is generally considered that the liquid outer core of the Earth is laterally homogeneous because there exists active current convection (e.g., [45]). To demonstrate whether any outer core structure affects the tomographic image of the Hawaiian mantle plume, we inverted both mantle and core phases for the 3-D mantle structure alone assuming that the outer core is laterally homogeneous (Fig. 7b). It is found that the pattern is the same for the mantle structures with and without the outer core structure to be inverted (Fig. 7a and b). Some differences in the amplitude of velocity anomaly exist in the middle and lower mantle. The model without the outer core structure shows a slightly larger amplitude (Fig. 7b). These results may be indicative of a trade-off between the mantle and outer core structures, which was pointed out by the previous studies (e.g., [23,28,29]).

4.2. Effect of the CMB topography

CMB is the most important boundary of the Earth's interior, exhibiting the strongest contrasts in density and chemical composition as well as seismic wave velocity. It is suggested that CMB has undulations of up to 10 km [34,35] due to hot materials pulling up and cold materials depressing in the mantle. Such large undulations would certainly affect the tomographic image because ray paths and travel times of PcP, Pdiff and core phases depend directly on the CMB topography. However, different disciplines suggested different CMB models. Even in the same dis-

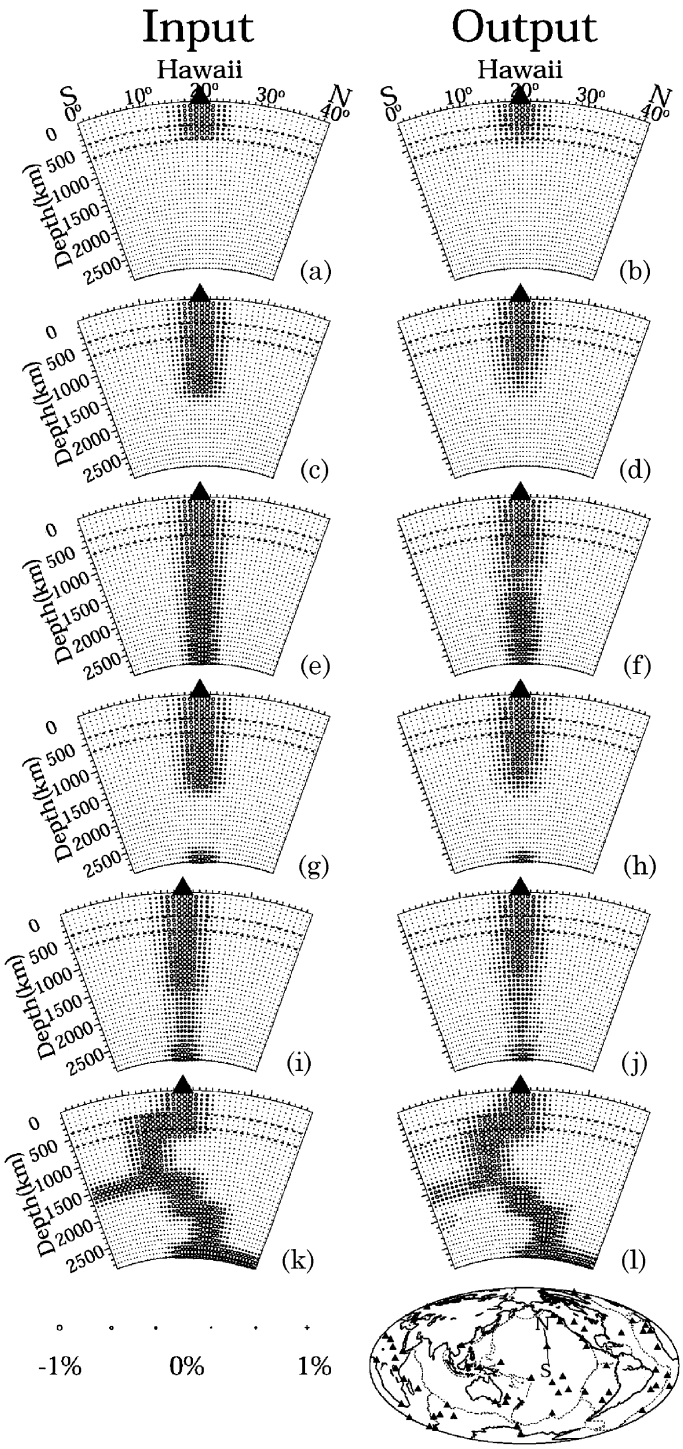

Fig. 9. Input models (left) and inverted results (right) of synthetic tests conducted. Circles and crosses denote slow and fast velocities, respectively. The velocity perturbation scale (in %) is shown at the bottom. Two dashed lines denote the 410 and 660 km discontinuities. Location of the profile is shown on the insert map. The triangles denote the hotspots in the world.

cipline (e.g., seismology), considerable differences exist, partly due to the different data sets and inversion techniques used.

In this work we used three CMB topographic models [33,46,35] to investigate their effects on the image of the Hawaiian mantle plume. These three CMB models

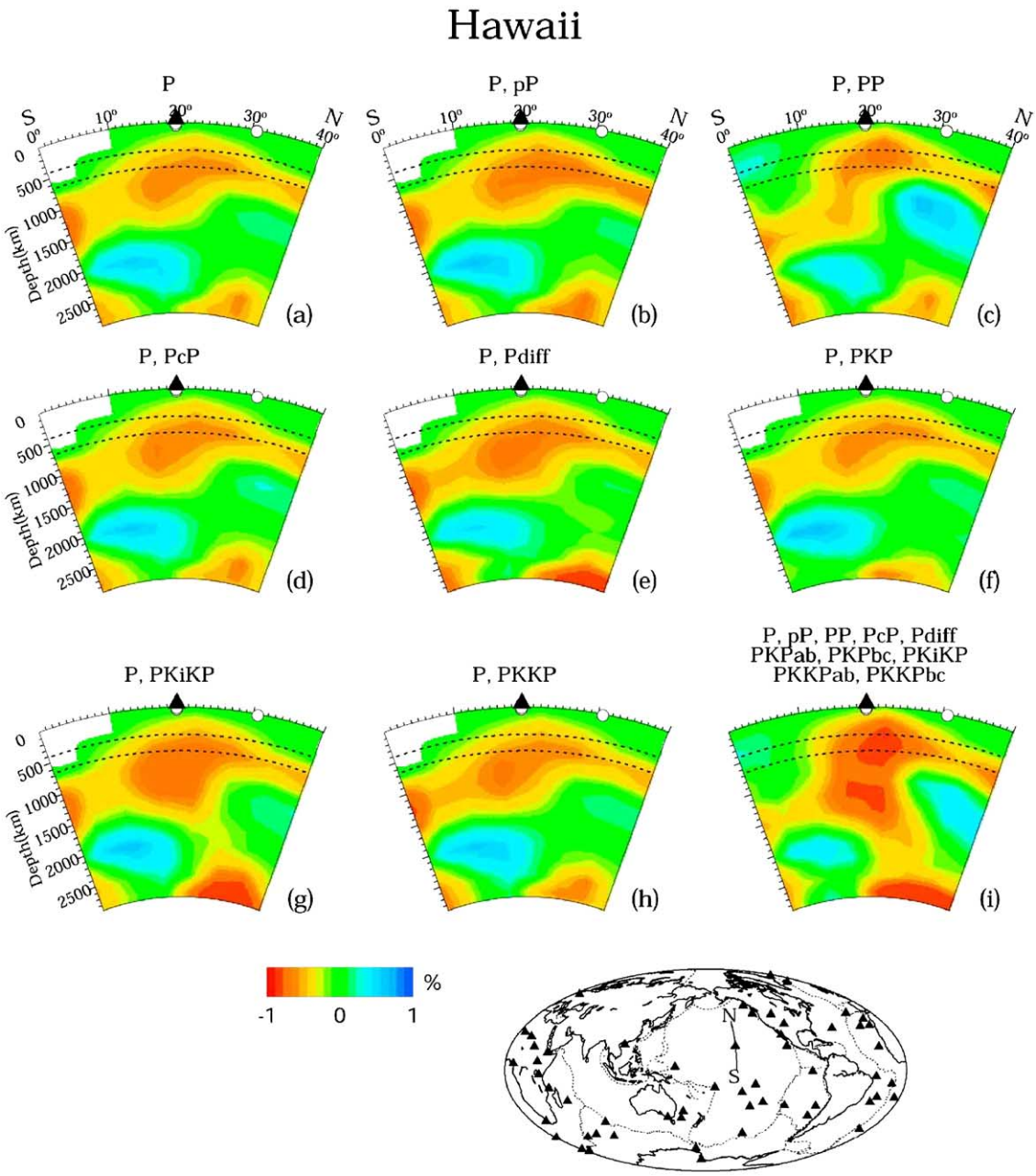

Fig. 10. P-wave tomographic images along the north–south vertical cross-section passing through the Hawaiian hotspot, obtained by using P and one kind of later phases. The CMB topography was not taken into account and the outer core structure was inverted jointly. The types of the rays used in the inversion are shown above each panel. Red and blue colors denote the low and high velocities, respectively. The velocity perturbation scale (in %) is shown at the bottom. The other labels are the same as those in Fig. 7.

show different overall pattern and topographic peaks of 6, 10 and 3 km, respectively. Of these three topographic models, the model of Morelli and Dziewonski [33] displays slight depression around the Hawaiian island chain, while that of Sze and van der Hilst [35] shows elevated topography around Hawaii, which is consistent with the low-V anomaly in the mantle. It is found that the tomographic results with and without the CMB topography show the same pattern of velocity anomalies: a continuous low-V anomaly below the Hawaii extends down to the CMB. Prominent differences exist in the amplitude below 2000 km depth, in particular, in the models with the CMB topography [33,35] (Fig. 7c and e), suggesting that further efforts should be

made to obtain a reliable CMB topographic model so that the Hawaiian mantle plume can be imaged better.

4.3. Effect of various seismic phases

To confirm how later phases affect the tomographic image, we conducted two series of tomographic inversions and the checkerboard resolution tests by using different data sets. One is to combine the direct P wave with one kind of later phases in the inversion (Figs. 10 and 11); the other is to add more kinds of later phases gradually in the inversion (Fig. 12). When the pP rays are included, the amplitude of velocity anomalies is changed beneath the Hawaiian hotspot above the middle mantle and in the lowermost mantle slightly (Fig. 10b or 12b). The changes in the pattern of the check-

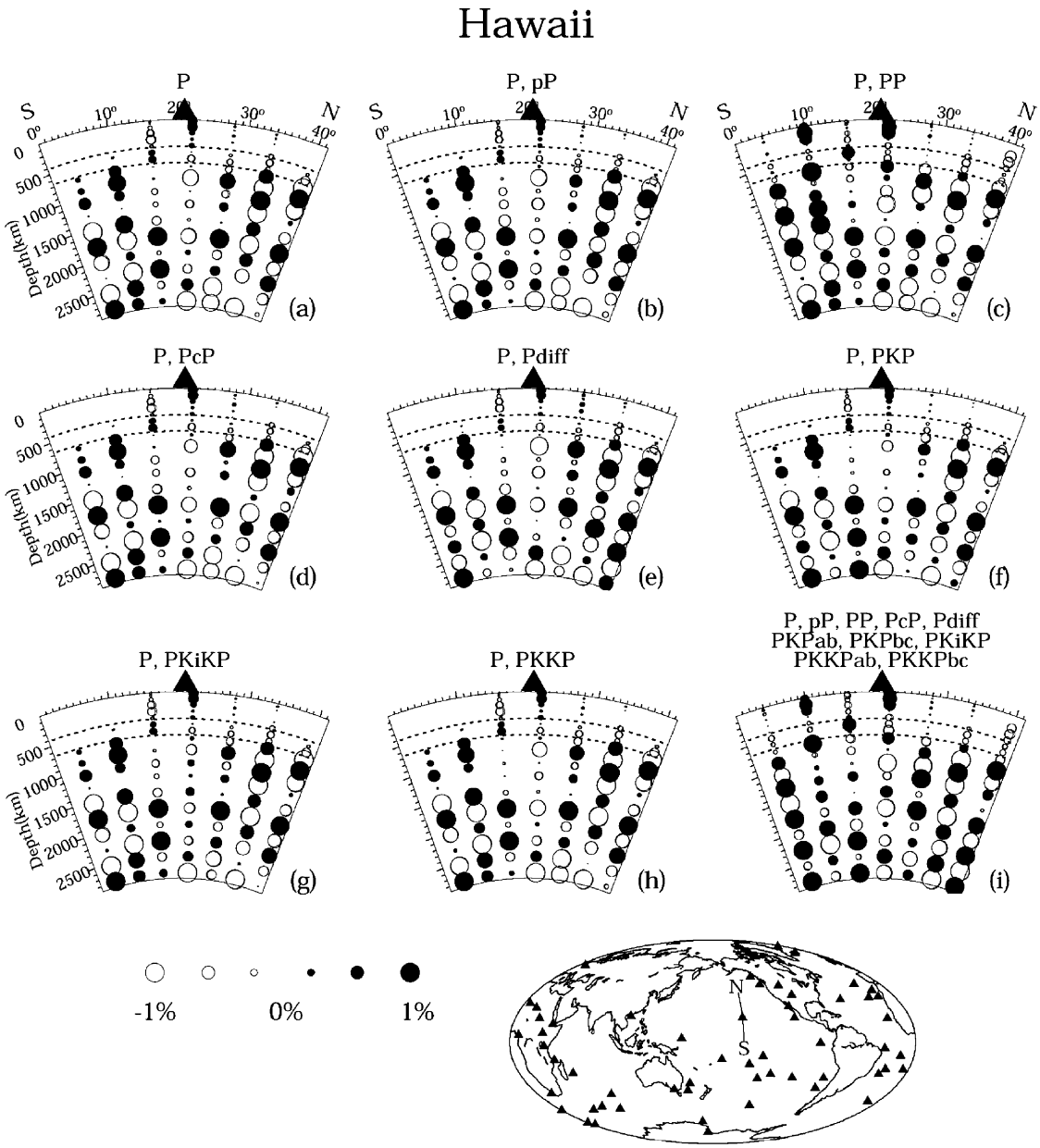

Fig. 11. Results of the checkerboard resolution tests along the north–south vertical cross-section by using the similar data sets as shown in Fig. 10. Open and solid circles denote the slow and fast velocities, respectively. The velocity perturbation scale is shown at the bottom. Two dashed lines denote the 410 and 660 km discontinuities, respectively. Location of the cross-section is shown at the bottom. Triangles denote the hotspots in the world.

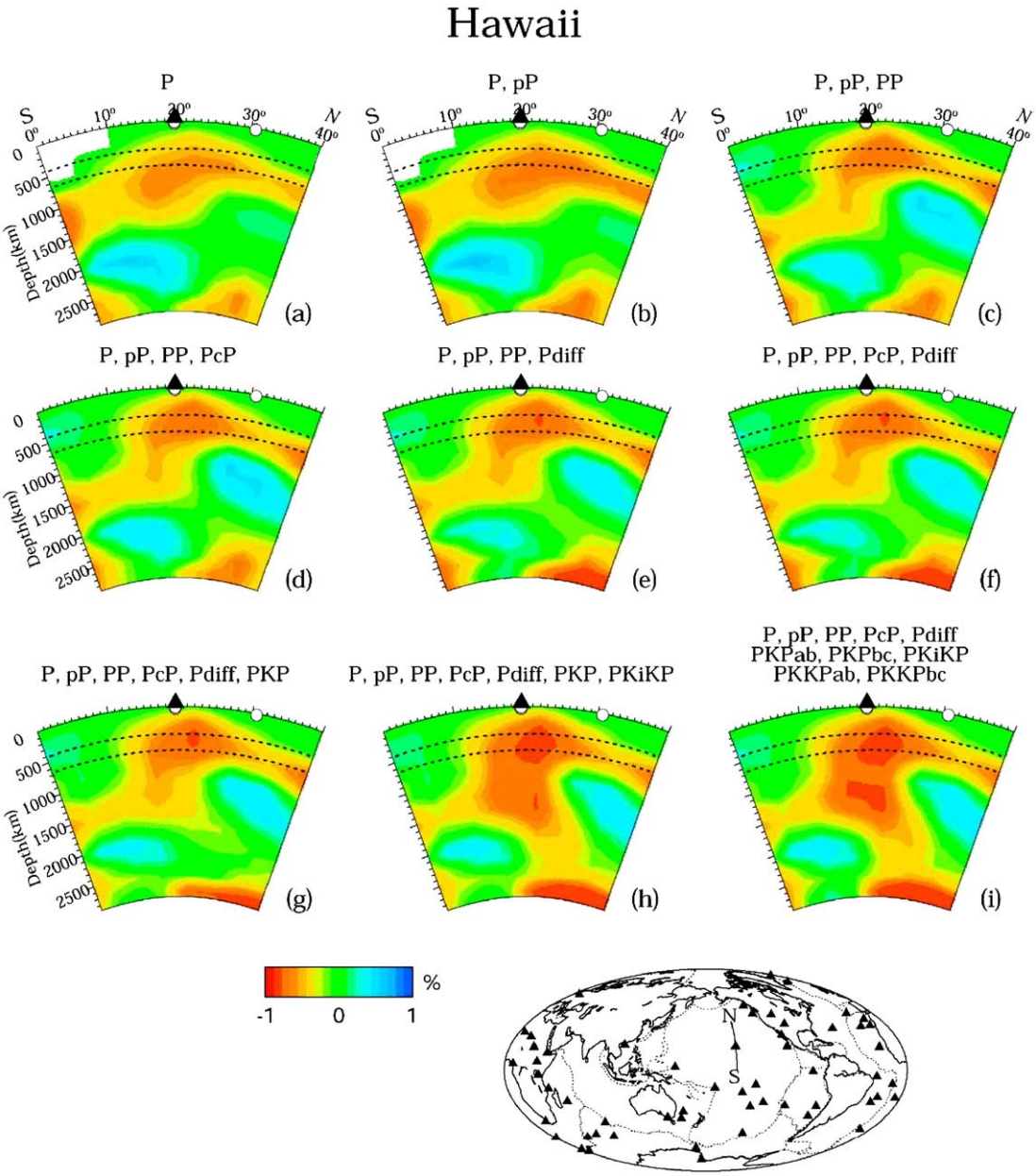

Fig. 12. The same as Fig. 10 but for P and more kinds of later phases.

erboard resolution tests cannot be found visually but the amplitude of anomalies is changed (Fig. 11a and b) because the pP phase has almost the similar ray path as the direct P wave (Fig. 5a, b, d and e). PP rays change the pattern of the image above 1700 km depth (Figs. 10c and 12c) because PP rays have a good coverage above the middle mantle (Fig. 5c and f). The checkerboard resolution tests also delineate some significant improvement at these depths though their pattern is not retrieved completely (Fig. 11c). When PcP rays are incorporated, both the pattern and amplitude of slow anomalies have almost no change (Figs. 10d and 12d), and the checkerboard resolution tests also show such similar features (Fig. 11d) because of few ray paths of PcP existing under Hawaii (Fig. 5g). Pdiff rays enhance the amplitude of slow anomalies above 1500 km depth and in the lowermost mantle (Figs. 10e and 12e). PKP rays reduce the amplitude of slow anomalies in the lowermost mantle (Figs. 10f and 12g). Such effects of both Pdiff and PKP rays can also be demonstrated in

the checkerboard resolution tests (Fig. 11e and f) and the distribution of travel time residuals (Fig. 4b and c) and ray paths (Fig. 5h and i). When PKiKP rays are added, the pattern of slow anomalies is changed in the entire mantle (Fig. 10g), their effect is more clearly visible in Fig. 12h after the combination of mantle phases and PKP phase. Such great contribution of PKiKP rays to the image of the Hawaiian mantle plume may be due to their quite different take-off angles compared to those of other phases (Fig. 5j), which can significantly improve the ray crisscrossing in the mantle under Hawaii. Another possibility is that there are some large and positive residuals amounting up to 4.0 s around of Hawaii (Fig. 4d). Furthermore, though there exist relatively smaller residuals northeast of Hawaii (Fig. 4d), many rays pass through there (Figs. 3d and 5j). The checkerboard resolution tests with PKiKP also reveal such significant improvement (Fig. 11g). When only P and PKKP rays are used, it is not easy to find the change visually (Fig. 10h). However, when all phases are used, it is clear that PKKP rays affect the amplitude of slow anomalies around 1500 km depth beneath Hawaii (Fig. 12h and i) and that a continuous low-V anomaly is imaged below the Hawaiian hotspot in the entire mantle (Fig. 10i or 12i). Such slight effect of PKKP may be due to some relatively large and positive residuals around Hawaii (Fig. 4e). The effect of PKKP can also be observed in the checkerboard resolution tests (Fig. 11h).

To further affirm whether PKiKP phases affect the image of the Hawaiian plume significantly, two more tomographic inversions are carried out with a new data set, which is extended to the year 2003 (Table 1). One is to use this new data set with all kinds of seismic phases (Fig. 13a). The other is to use the same data set but without PKiKP (Fig. 13b). The total number of the data is added to around 1.2 million in the new data set. Of all the data, the number of PKiKP is extended to over 9000 (Table 1). PKiKP rays have a better coverage (Fig. 13c and e) than those (Figs. 3d and 5j) in the original data set (1964–1998), and their residuals have a consistent pattern with those in the original data set (Figs. 4d and 13d). Our results show that there are no obvious changes in the pattern of velocity anomalies around Hawaii in the entire mantle, but the new data set still improves the image of the Hawaiian plume in the amplitude below 2000 km depth significantly (Figs. 12i and 13a), indicating that all the data available worldwide should be attempted to use in the global study. In addition, it is also found that there still exist some prominent differences in the lower mantle between two models with and without PKiKP, as shown in Figs. 10 and 12, implying that PKiKP indeed makes greater contributions to imaging the Hawaiian plume (Fig. 13).

These results suggest that later phases, PP, Pdiff, PKP and particularly PKiKP, play an important role in better constraining the mantle structure, and in gaining a new insight into the mantle plume under the Hawaiian hotspot. We cannot rule out the possibility that the continuous low-V anomaly beneath the Hawaiian hotspot is affected by the inevitable noises of later phase arrival time pickings in the ISC data set (e.g., [33,47]) though we have winnowed the data carefully, and also perhaps due to the error in the travel time calculation of the core phases, which are affected by the CMB and/or ICB (inner core boundary) topography, and the outer core structure. Nevertheless, we believe that this new image provides us vital information for better understanding the origin of the Hawaiian mantle plume.

4.4. Comparison with other models

The CMB source of the Hawaiian hotspot is commonly assumed, but the global tomographic studies exhibited quite different images. The models of Zhao [6,7] displayed intermittent low-V anomalies in the whole mantle, which have a pattern similar to Fig. 12f. Our present results exhibit a continuous low-V cylinder ascending from the hot thermal boundary layer, CMB, to the surface. Comparing to the previous models [6,7,24,25], the low-V anomaly is more localized in the upper mantle and greater in the uppermost lower mantle in our model (Figs. 7, 10i or 12i and 13a)). Such a significant improvement of the tomographic image of the Hawaiian plume, particularly for the middle mantle, is attributable to a large number of later phases used (Fig. 2). This image is also quite different from those showing low-V anomalies limited to the middle mantle and suggesting that the Hawaiian mantle plume is one branch of the south Pacific superplume (e.g., [24,25]), which shows an image similar to Figs. 10c and 12c. This may be due to the fact that they used a different data set, which has insufficient sampling and crisscrossing of rays below the middle mantle. Montelli et al. [8] used the finite-frequency tomographic method and suggested that the Hawaiian hotspot originates from the CMB. But their model shows very fewer low-V anomalies in the D'' region, perhaps owing to the limited kinds of later phases used (only pP and PP). Our present result shows the existence of a prominent low-V anomaly in the lowermost mantle under Hawaii, being consistent with the wave-

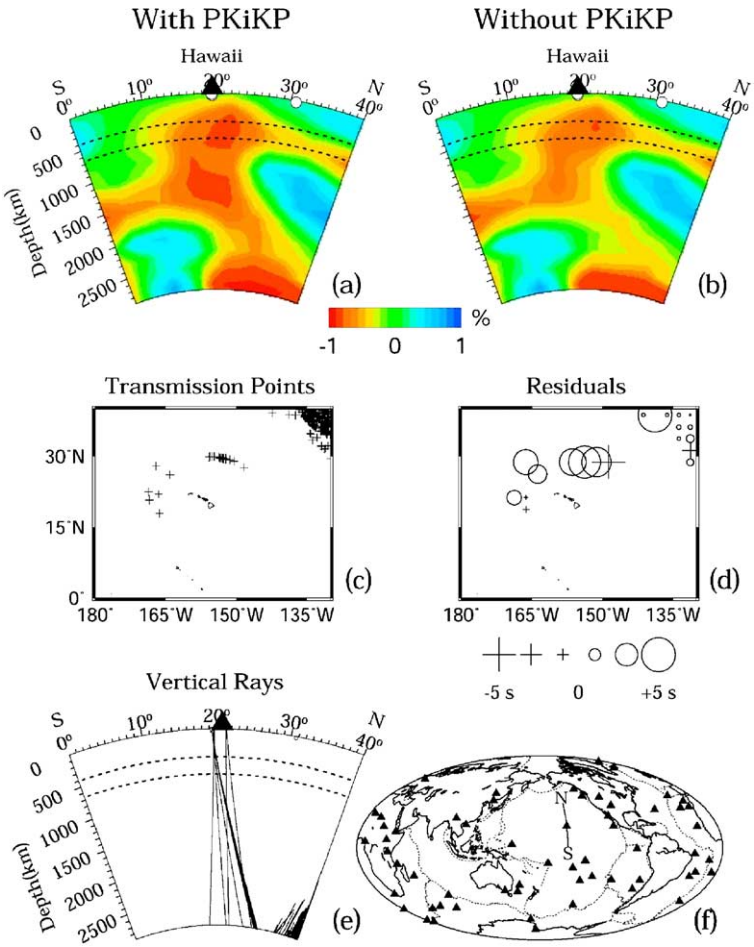

Fig. 13. (a) Tomographic images inferred from the data set extended to the year 2003 (Table 1); (b) the same as (a) but without PKiKP. Red and blue colors denote the low and high velocities, respectively. The scale for velocity anomalies (in %) is shown at the bottom of (a) and (b). The other labels in (a) and (b) are the same as those in Fig. 7. (c–e) Distributions of transmission points, travel time residuals and vertical seismic rays of PKiKP in this extended data set, respectively. Location of cross-section is shown in the insert (f). Crosses and circles in (d) denote the negative and positive residuals, respectively. The scale for residuals (in seconds) is shown at the bottom of (d). PKiKP rays have a better coverage than those (Figs. 3d and 5j) in the original data set (1964–1998) (Table 1) and their residuals have a consistent pattern with those (Fig. 4d) in the original data set. For details, see the text.

form modeling and recent tomographic results (e.g., [6,7,10,23]).

Our result also shows some differences from other results in the position of low-V anomaly at the CMB. Ji and Nataf [9] and Corrieu-Sipahimalani [48] suggested that the Hawaiian mantle plume would originate northwest of Hawaii, while Steinberger and O'Connell [49] predicted a source far south of Hawaii. Our results show that the plume source biases slightly towards the northeast (Fig. 6i), which is consistent with some of the recent tomographic results [7,23,27]. Our results are believed to be more reliable because a large number of later phases have been used in the inversion. The checkerboard resolution and synthetic tests (Figs. 8 and 9) all demonstrate that these features are robust.

The deflection of the Hawaiian mantle plume suggests that a non-stationary plume may be advected by prevailing mantle convection. Furthermore, this southward inclination of mantle plume beneath Hawaii (Figs. 7, 10i or 12i and 13a)) is also in agreement with the kinematic calculations [49,50]. At around 1500 km depth, a very weak slow anomaly extends southwards, which may represent some heat or material interchanges with the South Pacific superplume [7]. These features have been confirmed to be robust on the basis of a special synthetic test (Fig. 9k and l).

Although this study shows a well-resolved structure of the Hawaiian mantle plume with a diameter of about 800 km, rising from a broad root zone (>1400 km) and culminating in a plume with a diameter of up to about

1800 km (from middle to upper mantle) (Figs. 7, 10i or 12i and 13a)), the real diameter of the Hawaiian plume should be much smaller. Hence, continuing efforts should be made to deploy some ocean-bottom seismic stations around the Hawaiian island chain to improve the spatial resolution of the mantle structure to obtain a detailed structure of the Hawaiian plume.

5. Conclusions

We have fully investigated the influences of various mantle and core phases, the CMB topography and the outer core structure on the determination of 3-D mantle structure under the Hawaiian hotspot. Our results show that the CMB topography affects significantly the tomographic image of the Hawaiian plume below 2000 km depth, suggesting that further efforts should be made to obtain a reliable CMB model. Later phases often sample the mantle structure not usually sampled by the direct P waves, and we found that the later phases, PP, Pdiff, PKP and particularly PKiKP, can make greater contributions to better imaging the Hawaiian plume.

We presented the first image of a continuous plume below Hawaii in the whole mantle inferred by applying an updated technique of Zhao [7] to a large number of later phases. This image is improved notably over the previous models [6–8,24] in the entire mantle, in particular, in and below the middle mantle. Such a significant improvement provides us seismological evidence indicating that the Hawaiian hotspot indeed originates from the CMB. The plume is deflected southward, which is likely due to the mantle flow. This indicates that the position of the Hawaiian hotspot on the surface is not stationary, as evidenced by the paleomagnetic and numerical modeling studies (e.g., [49–51]).

Acknowledgments

This work was partially supported by the research grants (nos. B-11440134, S-12002006 and A-17204037) from the Japanese Ministry of Education and Science to D. Zhao. The authors are grateful to E.R. Engdahl for kindly providing his reprocessed ISC data set, and to A. Morelli, Y. Obayashi, E. Sze and R. van der Hilst for providing their CMB models. We thank A. Rodgers, T. Tsuchiya, T. Irifune, A. Yamada and K. Idehara for thoughtful discussion. All of the figures are made by using the GMT [52]. We greatly appreciate S. King and four anonymous referees for providing constructive comments and suggestions, which improved the manuscript.

References

[1] G. Davies, Ocean bathymetry and mantle convection: 1. Large-scale flow and hotspot, J. Geophys. Res. 93 (1988) 10467–10480.
[2] N. Sleep, Hotspots and mantle plumes: some phenomenology, J. Geophys. Res. 95 (1990) 6715–6736.
[3] V. Courtillot, A. Davaille, J. Besse, J. Stock, Three distinct types of hotspots in the Earth's mantle, Earth Planet. Sci. Lett. 205 (2003) 295–308.
[4] J. Wilson, A possible origin of the Hawaiian island, Can. J. Phys. 41 (1963) 863–868.
[5] W. Morgan, Convection plumes in the lower mantle, Nature 230 (1971) 42–43.
[6] D. Zhao, Seismic structure and origin of hotspots and mantle plumes, Earth Planet. Sci. Lett. 192 (2001) 251–265.
[7] D. Zhao, Global tomographic images of mantle plumes and subducting slabs: insight into deep Earth dynamics, Phys. Earth Planet. Inter. 146 (2004) 3–34.
[8] R. Montelli, G. Nolet, F. Dahlen, G. Masters, R. Engdahl, S. Hung, Finite-frequency tomography reveals a variety of plumes in the mantle, Science 303 (2004) 338–343.
[9] Y. Ji, H. Nataf, Detection of mantle plumes in the lower mantle by diffraction tomography: Hawaii, Earth Planet. Sci. Lett. 159 (1998) 99–115.
[10] S. Russell, T. Lay, E. Garnero, Seismic evidence for small-scale dynamics in the lowermost mantle at the root of the Hawaiian hotspot, Nature 396 (1998) 255–258.
[11] H. Nataf, Seismic imaging of mantle plumes, Annu. Rev. Earth Planet. Sci. 28 (2000) 391–417.
[12] A. Brandon, R. Walker, J. Morgan, M. Norman, H. Prichard, Coupled ^{186}Os and ^{187}Os evidence for the core–mantle interaction, Science 280 (1998) 1570–1573.
[13] G. Laske, J. Morgan, J. Orcutt, First results from the Hawaiian SWELL pilot experiment, Geophys. Res. Lett. 26 (1999) 3397–3400.
[14] M. Woods, E. Okal, Rayleigh-wave dispersion along the Hawaiian swell: a test of lithospheric thinning by the thermal rejuvenation at a hotspot, Geophys. J. Int. 125 (1996) 325–339.
[15] K. Priestley, F. Tilmann, Shear-wave structure of the lithosphere above the Hawaiian hot spot from two-station Rayleigh wave phase velocity measurements, Geophys. Res. Lett. 26 (1999) 1493–1496.
[16] X. Li, R. Kind, K. Priestley, S. Sobolev, F. Tilmann, X. Yuan, M. Weber, Mapping the Hawaiian plume conduit with receiver functions, Nature 405 (2000) 938–941.
[17] X. Li, R. Kind, X. Yuan, I. Wolbern, W. Hanka, Rejuvenation of the lithosphere by the Hawaiian plume, Nature 427 (2004) 827–829.
[18] J. Collins, F. Vernon, J. Orcutt, R. Stephen, Upper mantle structure beneath the Hawaiian swell: constraints from the ocean seismic network pilot experiment, Geophys. Res. Lett. 29 (2002), doi:10.1029/2001GL013302.
[19] C. Wolfe, S. Solomon, P. Silver, J. VanDecar, R. Russo, Inversion of body-wave delay times for mantle structure beneath the Hawaiian islands: results from the PELENET experiment, Earth Planet. Sci. Lett. 198 (2002) 129–145.
[20] S. Watson, D. Mckenzie, Melt generation by plumes: a study of Hawaiian volcanism, J. Petrol. 32 (1991) 501–537.
[21] N. Ribe, U. Christensen, The dynamical origin of the Hawaiian volcanism, Earth Planet. Sci. Lett. 171 (1999) 517–531.

[22] A. Hofmann, Mantle geochemistry: the message from oceanic volcanism, Nature 385 (1997) 219–229.
[23] H. Karason, R. van der Hilst, Tomograhic imaging of the lowermost mantle with differential times of refracted and diffracted core phases (PKP, Pdiff), J. Geophys. Res. 106 (2001) 6569–6587.
[24] Y. Fukao, A. To, M. Obayashi, Whole mantle wave tomography using P and PP-P data, J. Geophys. Res. 108 (2003), doi:10.1029/2001JB000989.
[25] M. Obayashi, T. Sakurai, Y. Fukao, Comparison of recent tomographic models (abstract), International Symposium on New Images of the Earth's Interior Through Long-Term Ocean-Floor Observations, Tokyo, Ocean Hemisphere Res. Cent., Tokyo, 1997, p. 29.
[26] J. Lei, D. Zhao, Global seismic tomography: on the effect of various mantle and core phases, Phys. Earth Planet. Inter. 154 (in press).
[27] R. van der Hilst, S. Widiyantoro, R. Engdahl, Evidence for deep mantle circulation from global tomography, Nature 386 (1997) 578–584.
[28] D. Vasco, L. Johnson, Whole Earth structure estimated from seismic arrival times, J. Geophys. Res. 103 (1998) 2633–2671.
[29] L. Boschi, A. Dziewonski, Whole Earth tomography from delay times of P, PcP and PKP phases: lateral heterogeneities in the outer core or radial anisotropy in the mantle? J. Geophys. Res. 105 (2000) 13675–13696.
[30] A. Morelli, A. Dziewonski, J. Woodhouse, Anisotropy of the inner core inferred from PKIKP travel times, Geophys. Res. Lett. 13 (1986) 1545–1548.
[31] J. Tromp, Inner core anisotropy and rotation, Annu. Rev. Earth Planet. Sci. 29 (2001) 47–69.
[32] R. Engdahl, R. van der Hilst, R. Buland, Global teleseismic earthquake relocation with improved travel times and procedures for depth determination, Bull. Seismol. Soc. Am. 88 (1998) 722–743.
[33] A. Morelli, A. Dziewonski, Topography of the core–mantle boundary and lateral heterogeneity of the liquid core, Nature 325 (1987) 678–683.
[34] A. Rodgers, J. Wahr, Inference of core–mantle boundary topography from ISC PcP and PKP travel times, Geophys. J. Int. 115 (1993) 991–1011.
[35] E. Sze, R. van der Hilst, Core mantle boundary topography from short period PcP, PKP, and PKKP data, Phys. Earth Planet. Inter. 135 (2003) 27–46.
[36] D. Zhao, A. Hasegawa, S. Horiuchi, Tomographic imaging of P and S wave velocity structure beneath northeastern Japan, J. Geophys. Res. 97 (1992) 19909–19928.
[37] D. Zhao, J. Lei, Seismic ray path variations in a 3D global velocity model, Phys. Earth Planet. Inter. 141 (2004) 153–166.
[38] J. Um, C. Thurber, A fast algorithm for two-point seismic ray tracing, Bull. Seismol. Soc. Am. 77 (1987) 972–986.
[39] B. Kennett, E. Engdahl, Travel times for global earthquake location and phase identification, Geophys. J. Int. 105 (1991) 429–465.
[40] B. Kennett, O. Gudmundsson, Ellipticity corrections for seismic phases, Geophys. J. Int. 127 (1996) 40–48.
[41] C. Paige, M. Saunders, LSQR: an algorithm for sparse linear equations and sparse least squares, Assoc. Comput. Math. Trans. Math. Software 8 (1982) 43–71.
[42] T. Tsuchiya, J. Tsuchiya, K. Umemoto, R. Wentzcovitch, Phase transition in $MgSiO_3$ perovskite in the earth's lower mantle, Earth Planet. Sci. Lett. 224 (2004) 241–248.
[43] M. Murakami, K. Hirose, K. Kawamura, N. Sata, Y. Ohishi, Post-perovskite phase transition in $MgSiO_3$, Science 304 (2004) 855–858.
[44] J. Lei, D. Zhao, P-wave tomography and origin of the Changbai intraplate volcano in Northeast Asia, Tectonophysics 397 (2005) 281–295.
[45] J. Stevenson, Limits on lateral density and velocity variations in the Earth's outer core, Geophys. J. R. Astron. Soc. 88 (1987) 311–319.
[46] M. Obayashi, Y. Fukao, P and PcP travel time tomography for the core–mantle boundary, J. Geophys. Res. 102 (1997) 17825–17841.
[47] O. Gudmundsson, J. Davies, R. Clayton, Stochastic of global travel time data: mantle heterogeneity and random errors in the ISC data, Geophys. J. Int. 102 (1990) 25–43.
[48] V. Corrieu-Sipahimalani, Modeles dynamiques du manteau terrstre: observations et contraintes, These de Doctorat en Sciences, University de Cergy-Pontoise, 1995.
[49] B. Steinberger, R. O'Connell, Advection of plumes in mantle flow: implications for hotspot motion, mantle viscosity plume distribution, Geophys. J. Int. 132 (1998) 412–434.
[50] B. Steinberger, Plumes in a convecting mantle: models and observations for individual hotspots, J. Geophys. Res. 105 (2000) 11127–11152.
[51] T. Tarduno, R. Cottrell, Paleomagnetic evidence for motion of the Hawaiian hotspot during formation of Emperor seamounts, Earth Planet. Sci. Lett. 153 (1997) 171–180.
[52] P. Wessel, W. Smith, New version of the Generic Mapping Tools (GMT) version 3.0 released, EOS Trans. AGU 76 (1995) 329.